Competition between exchange and magnetostatic energies in domain pattern transfer from BaTiO₃(111) to a Ni thin film

Kévin J. A. Franke [1], Colin Ophus [2], Andreas K. Schmid [2], and Christopher H. Marrows [1,*]

[1]*School of Physics and Astronomy, University of Leeds, Leeds LS2 9JT, United Kingdom*

[2]*National Center for Electron Microscopy, Molecular Foundry, Lawrence Berkeley National Laboratory, Berkeley, California 94720, USA*

We use spin-polarized low-energy electron microscopy to investigate domain pattern transfer in a multiferroic heterostructure consisting of a (111)-oriented BaTiO₃ substrate and an epitaxial Ni film. After *in situ* thick-film deposition and annealing through the ferroelectric phase transition, interfacial strain transfer from ferroelastic domains in the substrate and inverse magnetostriction in the magnetic thick film introduce a uniaxial in-plane magnetic anisotropy that rotates by $60°$ between alternating stripe regions. We show that two types of magnetic domain wall can be initialized in principle. Combining experimental results with micromagnetic simulations, we show that a competition between the exchange and magnetostatic energies in these domain walls has a strong influence on the magnetic domain configuration.

I. INTRODUCTION

Domain pattern transfer from (001)-oriented BaTiO₃ substrates into ferromagnetic thick films via interfacial strain transfer and inverse magnetostriction has been investigated intensively [1–6]. The multiferroic heterostructures thus obtained have been used to demonstrate electric-field-induced magnetization switching [1,5,6], magnetic domain-wall motion [7,8], and electric-field control of spin waves [9,10], thus holding the promise of low-power spintronic devices.

BaTiO₃ is a perovskite ferroelectric. Below $120°C$, the cubic parent phase transforms into a tetragonal phase with a lattice elongation along an edge ($\langle 001 \rangle$). This distortion is associated with a shift of the positively charged Ti^{4+} ions and negatively charge O^- ions in opposite directions, giving rise to an electric polarization parallel to the lattice elongation. Strain relaxation leads to the formation of ferroelastic/ferroelectric domains with a perpendicular orientation of the lattice elongation and associated polarization in adjacent domains [11,12].

Recently, we reported on domain pattern transfer from (111)-oriented BaTiO₃ substrates into Co thick films, where different $60°$ and $120°$ domain-wall structures are observed [13]. Here we investigate the imprinting of the ferroelectric domains of (111)-oriented BaTiO₃ substrates into thick epitaxial Ni films through a Pd buffer layer [14]. Crucially, Ni exhibits a lower saturation magnetization M_s than Co, resulting in a reduced importance of magnetostatic effects. Combining spin-polarized low-energy electron microscopy (SPLEEM) [15,16] with micromagnetic simulations, we show that the competition between exchange and magnetostatic energies has a significant (film-thickness-dependent) effect on the orientation of the magnetization in the magnetic domains.

II. FILM GROWTH AND IMAGING

Thick films were deposited in the SPLEEM instrument using molecular beam epitaxy. First, a Pd seed layer was deposited onto the BaTiO₃ substrate followed by the growth of a 3-nm-thick Ni layer, both at room temperature. It was no longer possible to observe any signal from the BaTiO₃ in the Auger spectra after the Pd layer was grown, meaning that it must be at least several nm thick. The in-plane magnetization components of the as-deposited film are shown in Fig. 1(a) for two orthogonal directions of magnetic contrast (indicated with double-headed arrows). The fact that SPLEEM imaging is possible relies on there being a crystalline film, and so our sample must be epitaxial. To determine the local magnetization direction, we take a series of images for various angles Ω of the in-plane contrast direction, set by the polarization axis of the spin source [16]. The normalized contrast m for the two largest domains as a function of Ω is shown as dots in Fig. 2(a).

The data correspond to the projection of the magnetization onto the contrast direction and are therefore fitted to $m = \cos(\Omega - \phi)$. The magnetization angle ϕ thus obtained is indicated by a radial line. The shaded area of the same color indicates the uncertainty. The local magnetization direction is also plotted with arrows of the same color in Fig. 1.

The domain pattern we observe in the as-deposited film [Fig. 1(a)] is somewhat random, but the magnetization aligns along a uniaxial direction with the magnetization rotating by $180°$ between neighboring domains. After heating the sample to $300°C$, well into the cubic phase, and returning to room temperature, the domain pattern changes significantly [Fig. 1(b)]: An image taken with the magnetic contrast in the horizontal direction (left) reveals a zigzag stripe pattern. An image taken with the contrast direction rotated by $49°$ (right) helps clarify the origin of this pattern. The magnetization aligns along a uniaxial direction that rotates by $60°$ between
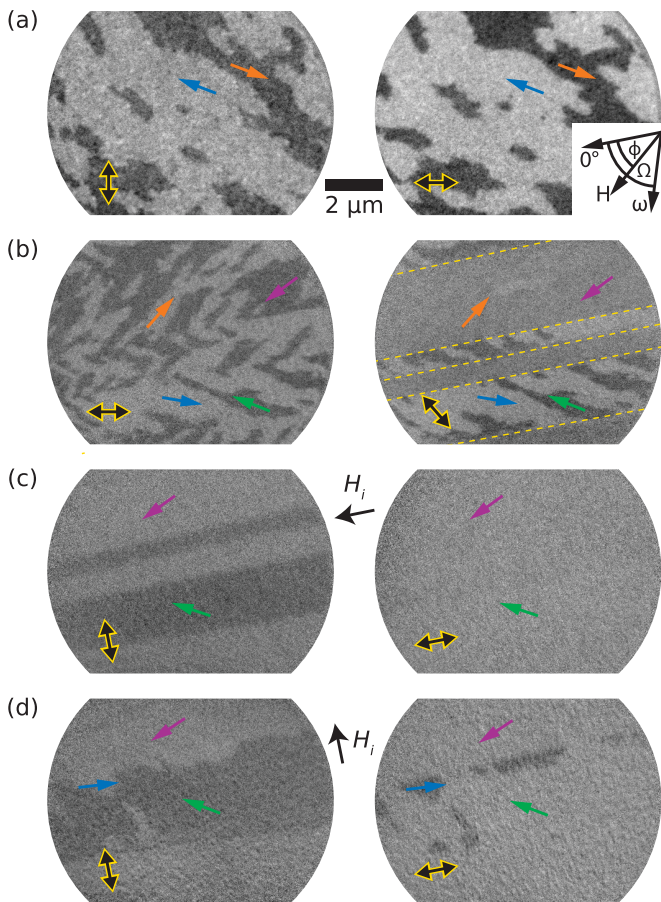
*c.h.marrows@leeds.ac.uk

FIG. 1. SPLEEM images of 3-nm-thick Ni film. Double-headed arrows indicate the axis of magnetic contrast and single-headed arrows show the local orientation of the magnetization. (a) After deposition of the film. (b) After annealing the sample. After application of an initializing magnetic field H_i, (c) parallel and (d) perpendicular to the stripe domains.

alternating stripe regions. Within these regions, a demagnetization pattern of domains separated by 180° domain walls is observed.

These images indicate the presence of a uniaxial anisotropy, the easy axis of which rotates by 60° between adjacent stripe regions, therefore forming domains of magnetic anisotropy as sketched in Fig. 3(a). This spatial modulation of the in-plane anisotropy is a result of coupling to ferroelastic domains in the ferroelectric substrate. When projected onto the (111) direction, the angle between the lattice elongations (discussed above) in adjacent ferroelastic domains is 60° [13]. Interfacial strain transfer from spatially modulated lattice elongations after heating the sample through the ferroelectric phase transition and inverse magnetostriction in the Ni film yield the anisotropy pattern observed here.

We apply an initializing magnetic field H_i, saturating the sample and then returning to remanence, along the anisotropy domains. As a result, the demagnetization pattern is erased and uniform magnetic domains are formed, as shown in Fig. 1(c). The spin rotation (i.e., difference in magnetization angle ϕ) between the two largest domains is $\Delta = 54 \pm 5°$, close to the 60° between anisotropy domains. We therefore conclude that the magnetization largely aligns with the
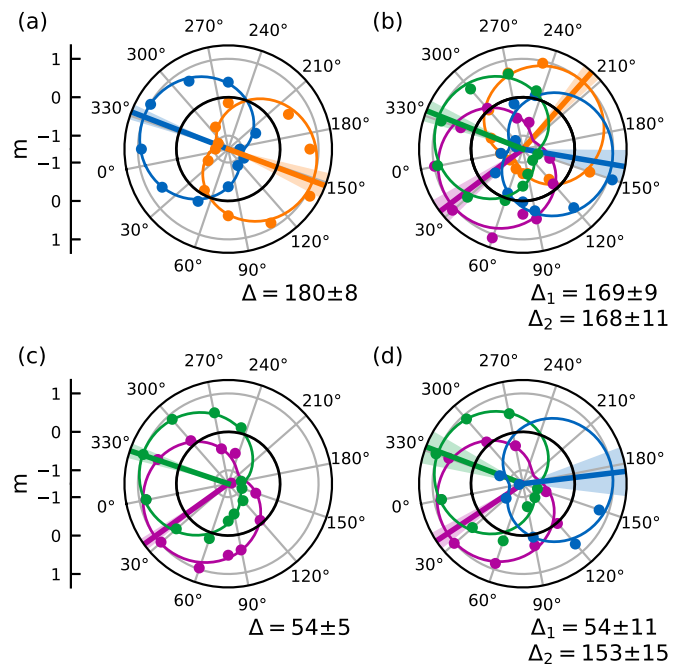

FIG. 2. Angular dependence of the normalized magnetic contrast corresponding to the images in Fig. 1. The data (dots) are compared to a fit (solid line). Radial lines indicate the resulting orientation of the magnetization with a transparent area indicating the uncertainty.

anisotropy directions. It forms the domain pattern sketched in Fig. 3(b), which has been labeled "60C," as the magnetization rotates by 60° between adjacent domains, and the domain wall is magnetically charged because of the accumulation of a net (virtual) magnetic charge due to the head-to-head (or tail-to-tail) magnetization configuration. Yet, significant deviations of the magnetization direction from the uniaxial anisotropy direction are observed. In particular, the narrow dark domain in Fig. 1(c) exhibits a lower contrast with its neighboring domains than the wider domain of similar contrast below.

The data shown in Fig. 1(c) were fitted using a nonlinear least-squares process to determine the spatial extent of the domains, using a custom MATLAB code. The fitting function m for each boundary is given by the sigmoid function,

$$m = \frac{r/r_0}{(1 + |r/r_0|^N)^{1/N}},$$

where r_0 sets the slope of the boundary at $r = 0$, and N defines a power law which controls how quickly the boundary tails decay. Each boundary function was scaled to the best-fit intensity levels of the domains on either side of each
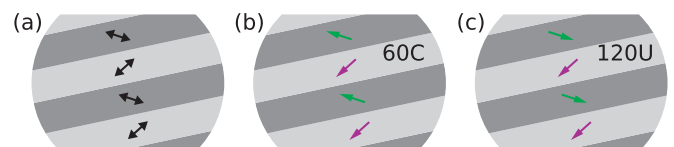

FIG. 3. (a) Schematic illustration of the magnetic anisotropy pattern induced by strain coupling to the (111)-oriented ferroelectric BaTiO$_3$ substrate. From this, two energetically distinct magnetization alignments are possible, as sketched in (b) and (c).
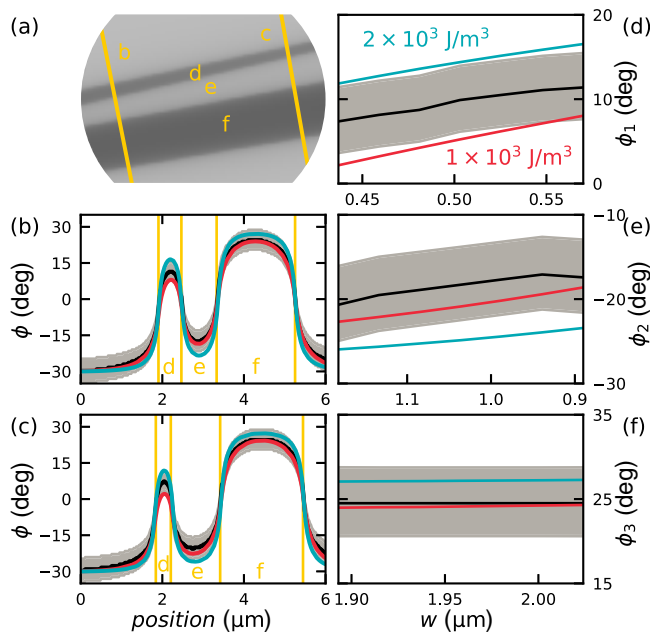
FIG. 4. Determination of the anisotropy constant: (a) Fit to the image in Fig. 1(c), as described in the main text. (b), (c) Profiles of the magnetization angle along the corresponding yellow lines in (a). The experimental data (black lines with gray shading indicating the uncertainty) are compared to micromagnetic simulations for a uniaxial anisotropy of $K_u = 1 \times 10^3$ and 2×10^3 J/m^3 (red and turquoise lines). (d)–(f) Magnetization angle ϕ at the center of the three central domains, labeled with the corresponding letter in (a), as a function of domain width w.

boundary. The best position r_{boundary} and rotation angle θ for all boundaries were fit simultaneously by parametrizing $(r = r' - r_{\text{boundary}}) \times \cos\theta$. The idealized domain pattern defined by these fitting results is shown in Fig. 4(a).

It can be observed that the domain walls are not perfectly parallel, i.e., the value of θ is not quite the same for all of them. This constitutes another indication that the magnetic domains are the result of strain coupling to ferroelectric domains in the BaTiO$_3$ substrate, as the latter exhibits domains that are separated by ferroelectric domain walls that deviate from being perfectly parallel [17].

Figures 4(b) and 4(c) show the profiles of the magnetization angles (black lines, with gray shading indicating the uncertainty) taken along the location of the yellow lines in Fig. 4(a). The profiles are subtly different due to the width of domains not being constant. For example, in Fig. 4(b), the domain labeled "d" is wider than in Fig. 4(c), while the domains labeled "e" and "f" are both narrower. Figures 4(d)–4(f) show the magnetization direction at the center of these three domains as a function of domain width. We do not observe a clear trend over this limited range of domains widths, but we compare the data in Figs. 4(b)–4(f) to micromagnetic simulations to estimate the magnitude of the uniaxial anisotropy.

III. MODELING AND ANALYSIS

We used OOMMF [18] to run numerical micromagnetic simulations with experimentally obtained parameters for the

film thickness, domain widths, and anisotropy directions. We use literature values for the saturation magnetization $M_s = 5.3 \times 10^5$ A/m and exchange stiffness $A = 8 \times 10^{-12}$ J/m [19,20].

The magnetization angles simulated for uniaxial anisotropy constants $K_u = 1 \times 10^3$ J/m^3 (red) and $K_u = 2 \times 10^3$ J/m^3 (turquoise) are compared to the experimental data in Figs. 4(b)–4(f). The experimental data mostly lie between the simulated data, and we conclude that the effective uniaxial anisotropy induced in the Ni film is $K_u = (1.5 \pm 5) \times 10^3$ J/m^3. This value is in line with results obtained for Ni films deposited at room temperature onto (001)-oriented BaTiO$_3$ substrates [4], and about an order of magnitude lower than the one obtained for Co on (111)-oriented BaTiO$_3$ [13].

After applying the initializing magnetic field H_i perpendicular to the anisotropy domains, one would expect the magnetization to align in the manner sketched in Fig. 3(c). That configuration is labeled "120U," as the magnetization rotates by 120° between adjacent domains, and the head-to-tail orientation does not yield a net magnetic charge, thus making the domain walls uncharged. However, this configuration does not correspond to the experimental observation shown in Fig. 1(d) [21]. We find that the 60C configuration is mostly initialized again, with a few regions [marked by a blue arrow in Fig. 1(d)] pointing in a direction perpendicular to the one the magnetic field was applied in.

This result is surprising for two reasons: first, the magnetization in one of the domains has switched by 180° from the direction it was initialized in by the applied magnetic field; second, the charged configuration is associated with a cost in magnetostatic energy over the uncharged configuration. One would thus expect the uncharged configuration to be initialized in Fig. 1(d), unless the increased contribution of the exchange energy of 120° domain walls over 60° domain walls exceeds the difference in magnetostatic energy. Clearly, in this sample, the 60C magnetization configuration is energetically favorable over the 120U one. Furthermore, the occurrence of regions with almost reversed magnetization [blue arrow in Fig. 1(d)] at the boundary with domains, making an angle of ≈150° with the magnetization in the domains, most likely reduces the magnetostatic energy.

The competition between exchange and magnetostatic energies is made more complex by the interaction between magnetic domain walls: the magnetization angle between neighboring domains is reduced as the domain width is decreased and the tails of domain walls overlap, as observed in Fig. 4. Previous articles have shown that charged and uncharged domain walls in multiferroic heterostructures exhibit different widths [13,22]. For a given spin rotation Δ, the width of an uncharged domain wall is $\delta_u \propto \sqrt{A/K_u}$, whereas for charged domain walls, the width $\delta_c \propto M_s^2 t/K_u$ depends on the film thickness t and the saturation magnetization of the material. Similarly, the energy of an uncharged domain wall $E_u \propto \sqrt{AK_u}$, while numerical simulations suggest that the energy E_c of charged domain walls roughly scales with $M_s^2 t$ [23–25].

These expressions give an indication of how the domain-wall widths and energies are expected to scale with the magnetic parameters and the film thickness. Crucially, we see
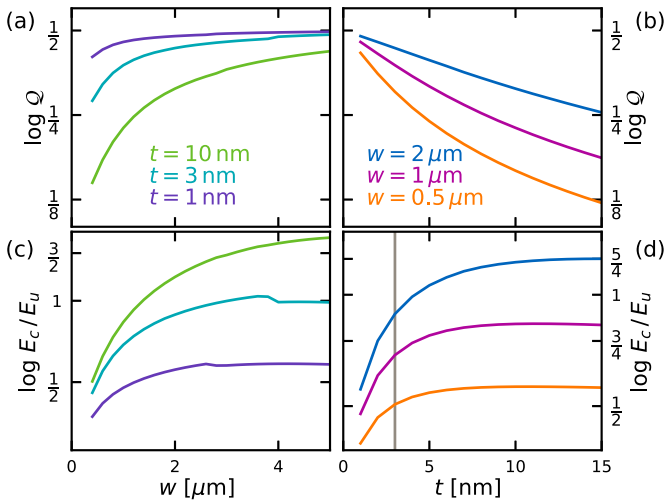
FIG. 5. Simulated dependence on (a) domain width and (b) film thickness of the ratio $\mathcal{Q} = \Delta_c/\Delta_u$. Colors correspond to different film thicknesses or domain widths, as indicated in the figure. (c), (d) Corresponding ratio between the energies of $60°$ charged and $120°$ uncharged configurations. The gray line indicates the 3 nm film thickness of the sample.

that for a large saturation magnetization M_s and film thickness t, magnetostatic effects lead to charged domain walls that are wider and higher in energy than uncharged domain walls. Conversely, here we investigate a film of small thickness t with low saturation magnetization M_s, where the domain-wall widths and energies are more comparable.

To compare the magnetization angles and energies of magnetization configurations in our sample, we use micromagnetic simulations once again, varying film thickness and domain width. Using the same parameters as above and two-dimensional periodic boundary conditions [26], we simulate regular stripe domains of equal widths. Simulations are initialized with the magnetization tilted by $45°$ from the stripe boundary towards the easy axes in the domains, such that the magnetization relaxes to the 60C or 120U configurations when the energy is minimized.

Figure 5(a) shows the ratio $\mathcal{Q} = \Delta_c/\Delta_u$ between spin rotations Δ of 60C and 120U configurations as a function of stripe width for three different film thicknesses. Similarly, Fig. 5(b) shows the effect of film thickness on $\mathcal{Q}$. For isolated domain walls, $\mathcal{Q} = 60°/120° = 1/2$. We see that for thick films and wide stripes, the data converge towards that value.

From the analytical expressions above, we know that the widths of the charged domain walls scale with the film thickness, while uncharged domain walls do not. As a result, domain-wall tails of charged domain walls increasingly overlap when the film thickness is increased, while the width of the charged domain walls remains unchanged. Generally, charged domain walls tend to be wider than uncharged ones, and thus overlap earlier when the domain width is reduced. Therefore, $\mathcal{Q}$ is reduced when the film thickness is increased or the domain width decreased.

The corresponding ratios between the energies of the 60C and 120U configurations are shown in Figs. 5(c) and 5(d).

We observe that for narrow domains in thick films, the 60C configuration is energetically favorable, but the ratio between energies increases as the domains widen or the film thickness is increased. For very thick films (1 nm) or narrow domains, the low-angle charged domain wall is always energetically favorable due to the lower exchange energy. For thick films (10 nm) and wide domains, the difference in magnetostatic energy overcomes the difference in exchange energy, and the larger angle but uncharged configuration becomes energetically favorable, in line with previous observations [13,22,25]. We also see that for an intermediate thickness (3 nm), both domain walls are energetically equivalent, i.e., the differences in exchange and magnetostatic energies balance. Hence we predict that by tuning the width of the domains or adjusting the film thickness, it will be possible to tune which configuration is the lower-energy magnetization state in this heterostructure.

IV. CONCLUSION

To conclude, we used SPLEEM combined with micromagnetic simulations to investigate domain pattern transfer in a multiferroic heterostructure consisting of a (111)-oriented $BaTiO_3$ substrate and an epitaxial Ni film. After *in situ* thick-film deposition and annealing through the ferroelectric phase transition, interfacial strain transfer from ferroelastic domains in the substrate and inverse magnetostriction in the magnetic thick film introduce a uniaxial in-plane magnetic anisotropy that rotates by $60°$ between alternating stripe regions. Two magnetization configurations, 60C and 120U, can be initialized in principle. Our micromagnetic modeling shows that a competition between exchange and magnetostatic energies can be used to tailor the energy landscape of magnetic configurations and to choose which configuration is energetically favorable by tuning domain widths and film thickness. This explains the unexpected appearance of 60C walls after applying an initializing magnetic field H_i perpendicular to the stripe regions in our experiments. We expect these result to be transferable to other systems with spatial modulations of the anisotropy.

The data associated with this paper are openly available from the University of Leeds Data Repository at Ref. [27].

[1] T. Lahtinen, J. Tuomi, and S. van Dijken, Pattern transfer and electric-field-induced magnetic domain formation in multiferroic heterostructures, Adv. Mater. **23**, 3187 (2011).

[2] T. H. E. Lahtinen, Y. Shirahata, L. Yao, K. J. A. Franke, G. Venkataiah, T. Taniyama, and S. van Dijken, Alternating domains with uniaxial and biaxial magnetic anisotropy in epitaxial Fe films on BaTiO$_3$, Appl. Phys. Lett. **101**, 262405 (2012).

[3] R. V. Chopdekar, V. K. Malik, A. Fraile Rodríguez, L. Le Guyader, Y. Takamura, A. Scholl, D. Stender, C. W. Schneider, C. Bernhard, F. Nolting, and L. J. Heyderman, Spatially resolved strain-imprinted magnetic states in an artificial multiferroic, Phys. Rev. B **86**, 014408 (2012).

[4] R. Streubel, D. Köhler, R. Schäfer, and L. M. Eng, Strain-mediated elastic coupling in magnetoelectric nickel/barium-titanate heterostructures, Phys. Rev. B **87**, 054410 (2013).

[5] Y. Shirahata, R. Shiina, D. L. González, K. J. A. Franke, E. Wada, M. Itoh, N. A. Pertsev, S. van Dijken, and T. Taniyama, Electric-field switching of perpendicularly magnetized multilayers, NPG Asia Mater. **7**, e198 (2015).

[6] M. Ghidini, F. Maccherozzi, X. Moya, L. C. Phillips, W. Yan, J. Soussi, N. Métallier, M. E. Vickers, N. J. Steinke, R. Mansell, C. H. W. Barnes, S. S. Dhesi, and N. D. Mathur, Perpendicular local magnetization under voltage control in Ni films on ferroelectric BaTiO$_3$ substrates, Adv. Mater. **27**, 1460 (2015).

[7] K. J. A. Franke, B. Van de Wiele, Y. Shirahata, S. J. Hämäläinen, T. Taniyama, and S. van Dijken, Reversible Electric-Field-Driven Magnetic Domain-Wall Motion, Phys. Rev. X **5**, 011010 (2015).

[8] D. López González, Y. Shirahata, B. Van de Wiele, K. J. A. Franke, A. Casiraghi, T. Taniyama, and S. van Dijken, Electric-field-driven domain wall dynamics in perpendicularly magnetized multilayers, AIP Adv. **7**, 035119 (2017).

[9] S. J. Hämäläinen, F. Brandl, K. J. A. Franke, D. Grundler, and S. van Dijken, Tunable Short-Wavelength Spin-Wave Emission and Confinement in Anisotropy-Modulated Multiferroic Heterostructures, Phys. Rev. Appl. **8**, 014020 (2017).

[10] H. Qin, R. Dreyer, G. Woltersdorf, T. Taniyama, and S. van Dijken, Electric-field control of propagating spin waves by ferroelectric domain-wall motion in a multiferroic heterostructure, Adv. Mater. **33**, 2100646 (2021).

[11] W. Merz, Domain formation and domain wall motions in ferroelectric BaTiO$_3$ single crystals, Phys. Rev. **95**, 690 (1954).

[12] D. Damjanovic, Ferroelectric, dielectric and piezoelectric properties of ferroelectric thin films and ceramics, Rep. Prog. Phys. **61**, 1267 (1998).

[13] K. J. A. Franke, C. Ophus, A. K. Schmid, and C. H. Marrows, 60° and 120° domain walls in epitaxial BaTiO$_3$(111)/Co multiferroic heterostructures, arXiv:2111.06191.

[14] Details of the in situ thin-film growth and imaging of magnetic contrast are described in Ref. [13].

[15] K. Grzelakowski and E. Bauer, A flange-on type low energy electron microscope, Rev. Sci. Instrum. **67**, 742 (1996).

[16] N. Rougemaille and A. K. Schmid, Magnetic imaging with spin-polarized low-energy electron microscopy, Eur. Phys. J. Appl. Phys. **50**, 20101 (2010).

[17] A. K. Tagantsev, L. E. Cross, and J. Fousek, *Domains in ferroic Crystals and Thin Films*, Vol. 13 (Springer, New York, 2010).

[18] M. Donahue and D. Porter, *OOMMF User's Guide, Version 1.0*, Interagency Report NISTIR No. 6376 (National Institute of Standards and Technology, Gaithersburg, MD, 1999).

[19] K. Niitsu, Temperature dependence of magnetic exchange stiffness in iron and nickel, J. Phys. D: Appl. Phys. **53**, 39LT01 (2020).

[20] J. Stöhr and H. Siegmann, *Magnetism: From Fundamentals to Nanoscale Dynamics* (Springer, New York, 2006).

[21] Images in Fig. 1(d) were taken in a different location than the ones shown in Fig. 1(c) because the same location could not be found again. Still, both sets of images are representative for the domain patterns observed throughout the sample.

[22] K. J. A. Franke, T. H. E. Lahtinen, and S. van Dijken, Field tuning of ferromagnetic domain walls on elastically coupled ferroelectric domain boundaries, Phys. Rev. B **85**, 094423 (2012).

[23] A. Hubert and R. Schäfer, *Magnetic Domains: The Analysis of Magnetic Microstructures* (Springer, New York, 1998).

[24] A. Hubert, Charged walls in thin magnetic films, IEEE Trans. Magn. **15**, 1251 (1979).

[25] K. J. A. Franke, D. López González, S. J. Hämäläinen, and S. van Dijken, Size Dependence of Domain Pattern Transfer in Multiferroic Heterostructures, Phys. Rev. Lett. **112**, 017201 (2014).

[26] W. Wang, C. Mu, B. Zhang, Q. Liu, J. Wang, and D. Xue, Two-dimensional periodic boundary conditions for demagnetization interactions in micromagnetics, Comput. Mater. Sci. **49**, 84 (2010).

[27] https://doi.org/10.5518/1304.